J|A|C|S
ARTICLES
Published on Web 04/07/2007

Spin-State Selective Carbon-Detected HNCO with TROSY Optimization in All Dimensions and Double Echo−Antiecho Sensitivity Enhancement in Both Indirect Dimensions

Kaifeng Hu, Beat Vögeli, and G. Marius Clore*

Contribution from the Laboratory of Chemical Physics, National Institute of Diabetes and Digestive and Kidney Diseases, National Institutes of Health, Bethesda, Maryland 20892-0520

Received November 13, 2006; E-mail: mariusc@intra.niddk.nih.gov

Abstract: A carbon-detected TROSY-optimized experiment correlating $^{1}H^{N}$, ^{15}N, and $^{13}C'$ resonances, referred to as c-TROSY−HNCO is presented, in which the $^{1}H^{N}$ and ^{15}N TROSY effects are maintained in both indirect dimensions, while the directly detected $^{13}C'$ is doubly TROSY-optimized with respect to $^{1}H^{N}$ and ^{15}N. A new strategy for sensitivity enhancement, the so-called double echo-antiecho (dEA), is described and implemented in the c-TROSY−HNCO experiment. dEA offers sensitivity enhancement of $\sqrt{2}$ in both indirect dimensions and is generally applicable to many multidimensional experiments. A carbon-detected HNCO experiment, c-HNCO, without TROSY optimization and sensitivity enhancement is also designed for comparison purposes. Relaxation simulations show that for a protein with a rotational correlation time of 10 ns or larger, the c-TROSY−HNCO experiment displays comparable or higher signal-to-noise (S/N) ratios than the c-HNCO experiment, although the former selects only 1/4 of the initial magnetization relative to the later. The high resolution afforded in the directly detected carbon dimension allows direct measurement of the doublet splitting to extract $^{1}J_{C^{\alpha}C'}$ scalar and $^{1}D_{C^{\alpha}C'}$ residual dipolar couplings. Simulations indicate that the c-TROSY−HNCO experiment offers higher precision (lower uncertainty) compared to the c-HNCO experiment for larger proteins. The experiments are applied to $^{15}N/^{13}C/^{2}H$/[Leu,Val]-methyl-protonated $IIB^{Mannose}$, a protein of molecular mass 18.6 kDa with a correlation time of ∼10 ns at 30 °C. The experimental pairwise root-mean-square deviation for the measured $^{1}J_{C^{\alpha}C'}$ couplings obtained from duplicate experiments is 0.77 Hz. By directly measuring the doublet splitting, the experiments described here are expected to be much more tolerant to nonuniform values of $^{1}J_{C^{\alpha}C'}$ (or $^{1}J_{C^{\alpha}C'} + {}^{1}D_{C^{\alpha}C'}$ for aligned samples) and pulse imperfections due to the smaller number of applied pulses in the "out-and-stay" coherence transfer in the c-HNCO−TROSY experiment relative to conventional ^{1}H-detected "out-and-back" quantitative *J* correlation experiments.

Introduction

Multidimensional ^{13}C-detected NMR spectroscopy[1−6] has recently attracted considerable attention as an alternative to ^{1}H-detected NMR spectroscopy for studying large macromolecules[7−10] and paramagnetic proteins.[11,12] These developments have been fueled in large part by progress in hardware technology, and in particular the advent of cryogenic probes optimized for ^{13}C detection.[13] ^{1}H-start/^{13}C-observe experiments[14] show particular promise for large macromolecules since they combine the advantages of high initial magnetization and reduced deuteron relaxation. Particularly useful are 3D HCC−TOCSY-type experiments designed for the assignment of side-chain ^{1}H and ^{13}C resonances.[9,10,15] Experiments correlating backbone ^{1}H, ^{15}N, and ^{13}C resonances, however, suffer from low signal-to-noise ratios owing to the long residence of ^{15}N and ^{13}C magnetization in the transverse plane.

The introduction of transverse relaxation-optimized spectroscopy (TROSY)[16] has extended the molecular mass range for ^{1}H-detected experiments from proteins of 40−50 kDa to ≥100 kDa.[17−20] In a single-quantum TROSY experiment, the transverse relaxation rate is reduced by selection of the slowly

(1) Maudsley, A. A.; Muller, L.; Ernst, R. R. *J. Magn. Reson.* **1977**, *28*, 463−469.
(2) Oh, B. H.; Westler, W. M.; Darba, P.; Markley, J. L. *Science* **1988**, *240*, 908−911.
(3) Chan, T. M.; Westler, W. M.; Santini, R. E.; Markley, J. L. *J. Am. Chem. Soc.* **1982**, *104*, 4008−4010.
(4) Bermel, W.; Bertini, I.; Duma, L.; Felli, I. C.; Emsley, L.; Pierattelli, R.; Vasos, P. R. *Angew. Chem., Int. Ed.* **2005**, *44*, 3089−3092.
(5) Bermel, W.; Bertini, I.; Felli, I. C.; Piccioli, M.; Pierattelli, R. *Prog. Nucl. Magn. Reson. Spectrosc.* **2006**, *48*, 25−45.
(6) Bermel, W.; Bertini, I.; Felli, I. C.; Kummerle, R.; Pierattelli, R. *J. Magn. Reson.* **2006**, *178*, 56−64.
(7) Eletsky, A.; Moreira, O.; Kovacs, H.; Pervushin, K. *J. Biomol. NMR* **2003**, *26*, 167−179.
(8) Bertini, I.; Felli, I. C.; Kummerle, R.; Moskau, D.; Pierattelli, R. *J. Am. Chem. Soc.* **2004**, *126*, 464−465.
(9) Hu, K. F.; Vogeli, B.; Pervushin, K. *J. Magn. Reson.* **2005**, *174*, 200−208.
(10) Jordan, J. B.; Kovacs, H.; Wang, Y. F.; Mobli, M.; Luo, R. S.; Anklin, C.; Hoch, J. C.; Kriwacki, R. W. *J. Am. Chem. Soc.* **2006**, *128*, 9119−9128.
(11) Bermel, W.; Bertini, I.; Felli, I. C.; Kummerle, R.; Pierattelli, R. *J. Am. Chem. Soc.* **2003**, *125*, 16423−16429.
(12) Bertini, I.; Luchinat, C.; Parigi, G.; Pierattelli, R. *ChemBioChem* **2005**, *6*, 1536−1549.
(13) Kovacs, H.; Moskau, D.; Spraul, M. *Prog. Nucl. Magn. Reson. Spectrosc.* **2005**, *46*, 131−155.
(14) Pervushin, K.; Eletsky, A. *J. Biomol. NMR* **2003**, *25*, 147−152.
(15) Hu, K. F.; Vogeli, B.; Clore, G. M. *J. Biomol. NMR* **2006**, *36*, 259−266.
(16) Pervushin, K.; Riek, R.; Wider, G.; Wuthrich, K. *Proc. Natl. Acad. Sci. U.S.A.* **1997**, *94*, 12366−12371.

relaxing doublet component of a spin *S*, scalar coupled to a spin *I* in the α or *β* state. For example, at a polarizing magnetic field of ∼1 GHz, the cross-correlated relaxation between the H^N-N dipolar interaction (DD) and the H^N or N chemical shift anisotropy (CSA) can almost completely cancel their autocorrelated relaxation for $^{15}N-^1H^N$ bonds. Two-dimensional (2D) [$^1H^N$,^{15}N]-TROSY can be implemented in most 3D triple-resonance experiments as a basic [$^1H^N$,^{15}N]-correlation element.[16,21−24] Concomitantly, ^{13}C relaxation can be significantly suppressed by deuteration of nonexchangeable protons.[25] The same TROSY principle reduces ^{13}C relaxation in aromatic $^{13}C-^1H$ bonds.[26] Recent implementations include methylene TROSY,[27] methyl TROSY,[28−30] and hNcaNH TROSY.[31] Relaxation optimization for methylene groups makes use of favorable interferences between $^1H-^{13}C$ and $^1H-^1H$ dipole and ^1H and ^{13}C CSA relaxation mechanisms.[27] Kay and co-workers have shown that the [^{13}C,^1H]-HMQC experiment is in fact a TROSY experiment for methyl groups due to cancellation of intra-methyl dipolar relaxation rates in large proteins such that the rapidly relaxing coherences do not mix with the slowly relaxing ones throughout the whole pulse sequence.[28,29] Using a [^{13}C,^1H]-HZQC experiment ($^{13}C/^1H$ zero-quantum) improves resolution even further.[30]

In this paper we present a novel ^1H-start/^{13}C-observe experiment, termed c-TROSY−HNCO, that is TROSY-optimized in all three dimensions correlating $^1H^N$, ^{15}N, and $^{13}C'$ resonances. To our knowledge, this represents the first time that both the [$^1H^N$,^{15}N]-TROSY building block is applied in the indirect dimensions and the directly detected $^{13}C'$ dimension is doubly TROSY-optimized with respect to $^1H^N$ and ^{15}N. The coherence transfer selecting TROSY components has been well demonstrated for biomacromolecules.[16−18,22,26,28,30] In addition, we employ a new strategy, the so-called double echo-antiecho (dEA), that provides $\sqrt{2}$ sensitivity enhancement in both indirect dimensions by coherence order selectivity (COS). The coherence order selective transfer throughout the experiment is obtained by concatenating a ST2-PT coherence transfer[32] from $^1H^N$ to ^{15}N and a with regard to ^{15}N "coherence order selective" to "spin-state selective" (COS-S^3) coherence transfer[33] from ^{15}N to directly detected $^{13}C'$. The design of the c-HNCO−TROSY experiment can serve as the basis for a large range of triple resonance ^{13}C-direct detection experiments. For example, the magnetization on the carbonyl carbon can be further transferred to the side-chain carbons for detection.[15] In addition, implementation of the dEA scheme represents a general concept for sensitivity enhancement.

Under most circumstances, ^1H-detect triple resonance experiments exhibit higher S/N than the corresponding ^{13}C-detect experiments. This includes the out-and-back ^1H-detected TROSY−HNCO which is one of the most sensitive triple resonance experiments. Nevertheless, there are certain situations in which the ^{13}C-detect triple resonance experiments are clearly superior—in particular under circumstances where the backbone amide ^1H_N resonances are selectively broadened relative to the ^{15}N and ^{13}C resonances. Examples of such situations include the presence of ^1H_N line broadening arising from water exchange or paramagnetic relaxation enhancement (either due to the presence of an intrinsic paramagnetic center or an extrinsic one added for other purposes). In general, protein NMR is usually carried out at pH values below 7 where backbone amide water exchange is slow. However, there are numerous examples of proteins that behave poorly (e.g., aggregate) at such pH values, necessitating the need to carry out NMR measurements at pH values ≥8. Likewise, any study on unfolded or partially folded proteins or proteins with large disordered regions will suffer from backbone amide ^1H_N exchange line broadening at pH values above around 7. It is under these types of conditions that ^{13}C-detect experiments come to the fore. In addition to these considerations, ^{13}C-detect experiments permit one to readily obtain high resolution in the ^{13}C dimension without impacting experimental measurement time. This is particularly useful, for example, in the measurement of $^{13}C-^{13}C$ couplings (e.g., $^1J_{C^\alpha C'}$ in HNCO experiments).

We show both experimentally, using a $^{15}N/^{13}C/^2H$/[Leu,Val]-methyl-protonated sample of $IIB^{Mannose}$ (18.6 kDa, $\tau_c \approx$ 10ns at 30 °C) as a test case, and theoretically from simulations that the S/N ratio for the c-TROSY−HNCO experiment is comparable to that of a regular carbon-detected HNCO experiment (c-HNCO) for systems with a rotational correlation time $\tau_c \geq$ 10 ns, although the former selects only a quarter of the initial magnetization. The high resolution afforded in the directly detected $^{13}C'$ dimension allows straightforward measurement of splittings arising from one-bond $C^\alpha-C'$ scalar couplings and, in an aligned medium,[34] residual dipolar couplings (RDC). Simulations indicate that, as the molecular weight of the macromolecule increases, the c-TROSY−HNCO experiment yields higher precision and therefore lower uncertainty in the measurement of the $C^\alpha-C'$ couplings than the c-HNCO experiment. In the case of $^{15}N/^{13}C/^2H$/[Leu,Val]-methyl-protonated $IIB^{Mannose}$ the experimental pairwise root-mean-square deviation (rmsd) for the measured $^1J_{C^\alpha C'}$ couplings is 0.77 Hz. It can be expected that the c-HNCO−TROSY experiment will be extremely useful for RDC measurements when the corresponding ^1H-detect experiment suffers sensitivity loss, due to rapid backbone amide water exchange or the presence of a paramagnetic center.

(17) Salzmann, M.; Wider, G.; Pervushin, K.; Wuthrich, K. *J. Biomol. NMR* **1999**, *15*, 181−184.
(18) Pervushin, K. *Q. Rev. Biophys.* **2000**, *33*, 161−197.
(19) Riek, R.; Pervushin, K.; Wuthrich, K. *Trends Biochem. Sci.* **2000**, *25*, 462−468.
(20) Tzakos, A. G.; Grace, C. R. R.; Lukavsky, P. J.; Riek, R. *Annu. Rev. Biophys. Biomol. Struct.* **2006**, *35*, 319−342.
(21) Salzmann, M.; Pervushin, K.; Wider, G.; Senn, H.; Wuthrich, K. *Proc. Natl. Acad. Sci. U.S.A.* **1998**, *95*, 13585−13590.
(22) Salzmann, M.; Wider, G.; Pervushin, K.; Senn, H.; Wuthrich, K. *J. Am. Chem. Soc.* **1999**, *121*, 844−848.
(23) Salzmann, M.; Pervushin, K.; Wider, G.; Senn, H.; Wuthrich, K. *J. Biomol. NMR* **1999**, *14*, 85−88.
(24) Yang, D. W.; Kay, L. E. *J. Biomol. NMR* **1999**, *13*, 3−10.
(25) Venters, R. A.; Farmer, B. T.; Fierke, C. A.; Spicer, L. D. *J. Mol. Biol.* **1996**, *264*, 1101−1116.
(26) Pervushin, K.; Riek, R.; Wider, G.; Wuthrich, K. *J. Am. Chem. Soc.* **1998**, *120*, 6394−6400.
(27) Miclet, E.; Williams, D. C.; Clore, G. M.; Bryce, D. L.; Boisbouvier, J.; Bax, A. *J. Am. Chem. Soc.* **2004**, *126*, 10560−10570.
(28) Ollerenshaw, J. E.; Tugarinov, V.; Kay, L. E. *Magn. Reson. Chem.* **2003**, *41*, 843−852.
(29) Tugarinov, V.; Hwang, P. M.; Ollerenshaw, J. E.; Kay, L. E. *J. Am. Chem. Soc.* **2003**, *125*, 10420−10428.
(30) Tugarinov, V.; Sprangers, R.; Kay, L. E. *J. Am. Chem. Soc.* **2004**, *126*, 4921−4925.
(31) Frueh, D. P.; Sun, Z. Y. J.; Vosburg, D. A.; Walsh, C. T.; Hoch, J. C.; Wagner, G. *J. Am. Chem. Soc.* **2006**, *128*, 5757−5763.
(32) Pervushin, K. V.; Wider, G.; Wuthrich, K. *J. Biomol. NMR* **1998**, *12*, 345−348.
(33) Lee, D.; Vogeli, B.; Pervushin, K. *J. Biomol. NMR* **2005**, *31*, 273−278.
(34) Tjandra, N.; Bax, A. *Science* **1997**, *278*, 1697−1697.

Experimental Section

$^{15}N/^{13}C/^{2}H]$/[Leu,Val]-methyl-protonated $IIB^{Mannose}$ (IIB^{Man}) of the *Escherichia coli* phosphotransferase system was expressed and purified as described previously.[15] The sample for NMR comprised 0.75 mM IIB^{Man} in 20 mM phosphate buffer, pH 6.5, containing 0.01% (w/v) sodium azide and 8% D_2O. Spectra were recorded at 30 °C on a Bruker AVANCE 800 MHz spectrometer equipped with a cryogenic *z*-gradient DUL $^{13}C\{^1H\}$ probe. $24(t_1) \times 40(t_2) \times 2048(t_3)$ complex points were acquired for both the 3D c-TROSY−HNCO and c-HNCO experiments with maximum acquisition times of 7 ms (H_N), 16.44 ms (^{15}N), and 127.8 ms ($^{13}C'$). The total experiment times for the c-TROSY−HNCO and c-HNCO experiments, recored with 40 scans per increment and an interscan delay of 0.8 s, were 44 and 42 h, respectively. The NMR data were processed using the program NMRPipe.[35] Note that the dataset for the 3D c-TROSY−HNCO is linearly recombined in both indirect dimensions prior to Fourier transformation due to the dEA acquisition mode. For better resolution along the ^1H dimension, linear prediction of size 36 was applied.

Results and Discussion

Description of the c-TROSY−HNCO Experiment. Figure 1A shows the experimental scheme for the 3D^{13}C-detected HNCO with TROSY optimization in all three dimensions, which we refer to hereafter as c-TROSY−HNCO. The initial ^1H polarization is excited by a 90° pulse on ^1H and generates transverse coherence (point *a*), which can be written in the single-transition operator basis as a linear combination of $\{(1/\sqrt{2})H_+N^{(\alpha)},(1/\sqrt{2})H_-N^{(\alpha)},(1/\sqrt{2})H_+N^{(\beta)},(1/\sqrt{2})H_-N^{(\beta)}\}$ (symbol in parentheses indicates the transition state of the spin), from which only the first term is selected through phase cycling to give the final NMR signal. The normalization factor is$(1)/(\sqrt{2})$. After ^1H constant time ($2T_1$) chemical-shift encoding, the corresponding density operator (point *b*) is:

$$\sigma_b = e^{-R_{H\pm N}(\alpha)\cdot 2T_1} \cdot e^{\pm i(\omega_H+\pi J_{HN})\cdot t_1}(1/\sqrt{2})H_-N^{(\alpha)} \qquad (1)$$

where the $e^{\pm i(\omega_H+\pi J_{HN})\cdot t_1}$ term represents the echo−antiecho quadrature detection in the ^1H dimension and $R_H\pm_{N^{(\alpha)}}$ is the transverse relaxation rate of the TROSY component in the ^1H dimension. $R_H\pm_{N^{(\alpha)}}$ can be expressed as $\Gamma^H_{DD,DD} + \Gamma^H_{CSA,CSA} + \Gamma^H_{DD,CSA}$, where $\Gamma^H_{DD,DD}$ and $\Gamma^H_{CSA,CSA}$ are the auto-correlated relaxation rates due to dipole−dipole (*DD*) interaction and chemical shift anisotropy (*CSA*), respectively, and $\Gamma^H_{DD,CSA}$ is the cross-correlated relaxation rate between *DD* and *CSA*. The following is the ST2-PT element,[32] which transfers the coherence to point *c*:

$$\sigma_c = e^{-R_{H\pm N}(\alpha)\cdot 2T_1} \cdot e^{\pm i(\omega_H+\pi J_{HN})\cdot t_1} \cdot \left(-\frac{1}{\sqrt{2}} \cdot iN_+H^{(\alpha)}\right) \qquad (2)$$

For simplification, relaxation during the transfer is not included here, and a detailed analysis of the relaxation is given in a following section. Subsequently, the ^{15}N chemical shift is encoded during the second constant time ($2T_2$) period, while the magnetization is transferred to C′ through *J*-coupling. The J_{NC^α} coupling is effectively refocused by applying a 180° pulse on C^α synchronized with the moving ^{15}N (ϕ_7) 180° pulse (see Figure 1 legend). At point *d*

$$\sigma_d = e^{-R_{N\pm H}(\alpha)\cdot 2T_2} \cdot e^{\pm i(\omega_N+\pi J_{HN})\cdot t_2} \cdot e^{-R_{H\pm N}(\alpha)\cdot 2T_1} \cdot e^{\pm i(\omega_H+\pi J_{HN})\cdot t_1}\left(-\frac{1}{\sqrt{2}} \cdot N_-C_zH^{(\alpha)}\right) \qquad (3)$$

where the $e^{\pm i(\omega_N+\pi J_{HN})\cdot t_2}$ term represents the echo−antiecho quadrature detection in the ^{15}N dimension and $R_{N\pm H^{(\alpha)}}$ is the transverse relaxation rate of the ^{15}N TROSY component. $R_{N\pm H^{(\alpha)}}$ can be expressed as $\Gamma^N_{DD,DD} + \Gamma^N_{CSA,CSA} + \Gamma^N_{DD,CSA}$, where $\Gamma^N_{DD,DD}$, $\Gamma^N_{CSA,CSA}$, and $\Gamma^N_{DD,CSA}$ are defined similarly to their ^1H

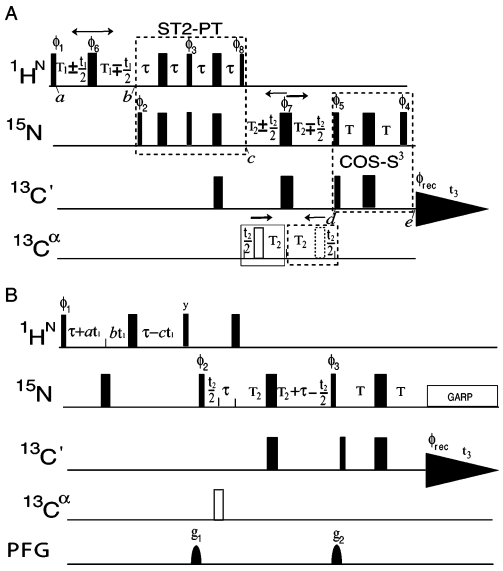

Figure 1. Pulse sequences for (A) the carbon-detected 3D c-TROSY−HNCO experiment and (B) the carbon-detected 3D c-HNCO experiment. The radio frequency pulses on $^{13}C'$, ^1H, and ^{15}N are applied at 174 ppm (58 ppm for C^α by setting the offset to −116 ppm), 8.5, and 118 ppm, respectively. Narrow and wide bars on the ^1H and ^{15}N channels indicate nonselective 90° and 180° pulses, respectively. To have null excitation on each other 90° and 180° pulses for $^{13}C'$ and C^α are set to 42 and 37 μs, respectively.. Unless indicated otherwise, all radio frequency pulses are applied with phase *x*. The delays have the following values: $\tau = 1/(4J_{HN}) = 2.65$ ms, $T = 1/(4J_{NC'}) = 17.5$ ms. In (A), the constant time periods T_1 and T_2 can be set according to the desired resolution in the ^1H and ^{15}N dimensions, bearing in mind relaxation considerations and INEPT transfer efficiency (here $T_1 = 3.5$ ms, $T_2 = 10.0$ ms). The phase cycle is: $\phi_1 = \{y, -x, y, -x\}$; $\phi_2 = \{-y\}$; $\phi_3 = \{-y, -y, -y, -y, y, y, y, y\}$; $\phi_4 = \{-y, -y, -x, -x\}$; $\phi_5 = \{x, x, y, y\}$; $\phi_6 = \{x, y, -x, -y\}$; $\phi_7 = \{x\}$; $\phi_8 = \{x, x, x, x, -x, -x, -x, -x\}$; $\phi_{rec} = \{y, -x, x, y, -y, x, -x, -y\}$. Quadrature detection in both $^1H(t_1)$ and $^{15}N(t_2)$ dimensions is achieved by the echo-antiecho method through shifting the 180° pulses on ^1H (ϕ_6) and ^{15}N (ϕ_7) forward and backward for each time increment point, respectively, as indicated by the arrows. Note, to refocus J_{NC^α} evolution, the 180° pulse on C^α during the ^{15}N constant time is synchronized with the moving ^{15}N 180° (ϕ_7) pulse; that is the pulses on C^α are alternately applied, as in the rectangular box when the ^{15}N 180° (ϕ_7) pulse is moving forward (thick arrow) and as in the dashed rectangular box when the ^{15}N 180° (ϕ_7) pulse is moving backward (thin arrow). In (B), the ^1H chemical shift is encoded during a semiconstant time period with effective evolution time $2at_1$ by setting $a = b + c$. The constant time period T_2 can be set according to the desired resolution in the ^{15}N dimension bearing in mind relaxation considerations and INEPT transfer efficiency (here $T_2 = 10.0$ ms). The 180° pulse on C^α is applied during the ^{15}N constant time to refocus J_{NC^α} evolution. The phase cycle is: $\phi_1 = \{x, -x\}$; $\phi_2 = \{x, x, -x, -x\}$; $\phi_3 = \{x, x, x, x, -x, -x, -x, -x\}$; $\phi_{rec} = \{x, -x, -x, x, -x, x, x, -x\}$. Pulsed field gradients indicated on the line marked PFG are applied along the *z*-axis with durations and strengths as follows: g_1, 600 μs and 30 G/cm; g_2, 900 μs and 30 G/cm. Quadrature detection in the $^1H(t_1)$ and $^{15}N(t_2)$ dimensions is achieved using States-TPPI[46] applied to the phases ϕ_1 and ϕ_2, respectively, together with ϕ_{rec}.

(35) Delaglio, F.; Grzesiek, S.; Vuister, G. W.; Zhu, G.; Pfeifer, J.; Bax, A. *J. Biomol. NMR* **1995**, *6*, 277−293.

dimension counterparts. The final element in the dashed rectangular box of the pulse scheme with phases ϕ_4 and ϕ_5 transfers magnetization from ^{15}N to ^{13}C′ for direct detection. This element performs "coherence order selective" to "spin-state selective" (COS-S^3)[33] transfer with regard to ^{15}N, thereby yielding the final magnetization $-[1/(\sqrt{2})]C\_H^{(\alpha)}N^{(\beta)}$ (point e). Without applying any decoupling during detection, the detected NMR signals can be written as:

$$\sigma_e = e^{-\overline{R_{C-H(\alpha)N(\beta)}^{C\alpha}}\cdot t_3 + i(\omega_{C'} - \pi^1 J_{NC'} + \pi^2 J_{HC\pm\pi^1 JC\alpha C')\cdot t_3} \cdot e^{-R_{N\pm H}(\alpha)\cdot 2T_2} \cdot e^{\pm i(\omega_N + \pi J_{HN})\cdot t_2} \cdot e^{-R_{H\pm N}(\alpha)\cdot 2T_1} \cdot e^{\pm i(\omega_H + \pi J_{HN})\cdot t_1} \cdot \left(-\frac{1}{\sqrt{2}} \cdot C\_H^{(\alpha)}N^{(\beta)}\right) \quad (4)$$

Thus, a clear doublet pattern is expected for carbonyl resonances at frequencies of $\omega_{C'} - \pi^1 J_{NC'} + \pi^2 J_{HC'} \pm \pi^1 J_{C^\alpha C'})$ due to J-coupling to C$^\alpha$ while under a single spin state with respect to both ^{15}B (β state) and ^{1}H^N (α state). $R_{C-H(\alpha)N(\beta)}^{C\alpha}$ is the transverse relaxation rate of ^{13}C′ doubly TROSY-optimized with respect to ^{1}H^N and ^{15}N. Briefly, using single-transition product operator notation, the relevant coherence transfer pathway can be described as:

$$H_z \xrightarrow{90^\circ_Y} \frac{1}{\sqrt{2}} H_+N^{(\alpha)}(a) \xrightarrow{180^\circ_{\phi 6}, 2T_1} \frac{1}{\sqrt{2}} H\_N^{(\alpha)}(b) \xrightarrow{\text{ST2-PT}} - \frac{1}{\sqrt{2}} iN_+H^{(\alpha)}(c) \xrightarrow{180^\circ_{\phi 7}, 2T_2} - \frac{1}{\sqrt{2}} 2N\_C_zH^{(\alpha)}(d) \xrightarrow{COS\text{-}S^3} - \frac{1}{\sqrt{2}} C\_H^{(\alpha)}N^{(\beta)}(e) \quad (5)$$

Selection of the doubly TROSY optimized component with regard to these two nuclei offers narrowing of line width compared to the conventional nonselective detection under decoupling.

It is worth noting that sensitivity enhancement can usually only be achieved in the indirect dimension immediately preceding the directly detected dimension. Here, for the first time, we show that sensitivity enhancement of $\sqrt{2}$ in both indirect dimensions can be obtained using the double echo–antiecho (dEA) scheme. We considered applying sensitivity enhancement in only the H_N (t_1) dimension and removing coherence order selectivity in the ^{15}N (t_2) dimension (i.e., without sensitivity enhancement in the ^{15}N (t_2) dimension). This would result in loss of spin-state selectivity for ^{15}N, and ^{15}N decoupling would then be applied during carbon detection (t_3 dimension). Without considering the effects of relaxation, this scheme should in principle be $\sqrt{2}$ more sensitive than the dEA scheme. However, because the coherence on H_N cannot be directly transferred to the directly detected carbon (since the H_N dimension does not immediately precede the directly detected dimension), the removal of coherence order selection (COS) in the t_2 dimension will inevitably result in loss of the COS property in the t_1 dimension; that is, sensitivity enhancement will actually be lost in both the t_1 and t_2 dimensions, rather than only in the t_2 dimension. Removal of the sensitivity enhancement scheme in the pulse sequence in Figure 1A will therefore effectively result in the non-TROSY version of the carbon-detected HNCO experiment presented in Figure 1B.

Chemical Shifts and Experimental Signal-to-Noise Ratio for the 3D c-TROSY–HNCO. For comparison purposes, a non-TROSY optimized carbon-detected HNCO experiment, c-HNCO (Figure 1B), was run as reference, in which there is no spin-state selectivity in any dimension and conventional decoupling on ^{15}N (and ^{1}H) is applied during detection. Figure 2A shows a schematic representation of the position of a cross-peak in the 3D c-TROSY–HNCO experiment (black) relative to that in the 3D c-HNCO one (red). There are offsets of $+J_{HN}/2$, $-J_{HN}/2$ (H$^{(\alpha)}$ state), (note γ_N is negative) and $-{}^1J_{NC'}/2 + {}^2J_{HC'}/2$ in H^N, N, and C′ dimensions, respectively, corresponding to the N$^{(\alpha)}$, H$^{(\alpha)}$, and N$^{(\beta)}$/H$^{(\alpha)}$ states, while chemical shifts are encoded in these three dimensions in 3D c-TROSY–HNCO. A selected region of the experimental spectra obtained for ^{15}N/^{13}C/^{2}H/[Leu,Val]-methyl-protonated IIB^{Man} ($\tau_c \approx 10$ ns at 30 °C) is analyzed in panels B–G of Figure 2. Cross-peaks arising from the H^N–N(Asp159)–C′(Thr158) correlation are viewed in three orthogonal planes, C′–H^N (Figure 2B), C′–N (Figure 2C), and H^N–N (Figure 2D), and clearly illustrate the positions and relative shifting of the cross-peaks in all three dimensions of the 3D c-TROSY–HNCO spectrum (black) relative to those in the 3D c-HNCO spectrum (red). One-dimensional slices from the two spectra taken through the H^N–N(Asp159)–C′(Thr158) cross-peaks (indicated by the dashed lines in Figure 2, B, C, and D) along the directly detected C′ dimension (Figure 2E), and the indirectly detected H^N (Figure 2F) and N (Figure 2G) dimensions, are aligned. Dashed lines in Figure 2E denote the peak intensities in the 3D c-TROSY–HNCO (black) and 3D c-HNCO (red) after normalization of the noise level, demonstrating that the experimental S/N ratios for the two spectra are comparable.

Under most circumstances, the c-HNCO–TROSY will generally have a lower S/N ratio than the conventional ^{1}H-detect TROSY–HNCO experiment.[36] For the 0.75 mM IIB^{Man} sample in 20 mM phosphate buffer, pH 6.5, the average estimated S/N loss is about a factor of 2 to 4 (see Figure S2 in the Supporting Information). However, the c-HNCO–TROSY can be extremely useful for the measurement of C$^\alpha$–C′ one-bond scalar and residual dipolar couplings under conditions where the ^{1}H-detect experiment suffers severe sensitivity loss due, for example, to extensive ^1H_N line broadening arising from rapid water exchange or the presence of a paramagnetic center with an isotropic **g** tensor. Note that for the measurement of C$^\alpha$–C′ one-bond scalar and residual dipolar couplings, a truly fair comparison between carbon- and proton-detected HNCO experiments requires that similar high resolution in the carbonyl dimension be obtained. This necessitates a significant increase in the number of points in the indirectly detected C′ dimension with a concomitant increase in measurement time for the ^{1}H-detected TROSY–HNCO.

In addition, we note that the nonconstant time nature of the ^{1}H-detect TROSY–HNCO in both the ^1H_N and C′ indirect dimensions is an important contributory factor to its high sensitivity. In contrast, the carbon-detect c-TROSY–HNCO experiment presented in Figure 1A uses constant time evolution in both the ^1H_N and ^{15}N dimensions that optimizes resolution while sacrificing signal-to-noise. However, modifying the ^1H_N (t_1) constant time evolution period for the c-TROSY–HNCO

(36) Yang, D. W.; Venters, R. A.; Mueller, G. A.; Choy, W. Y.; Kay, L. E. *J. Biomol. NMR* **1999**, *14*, 333–343.

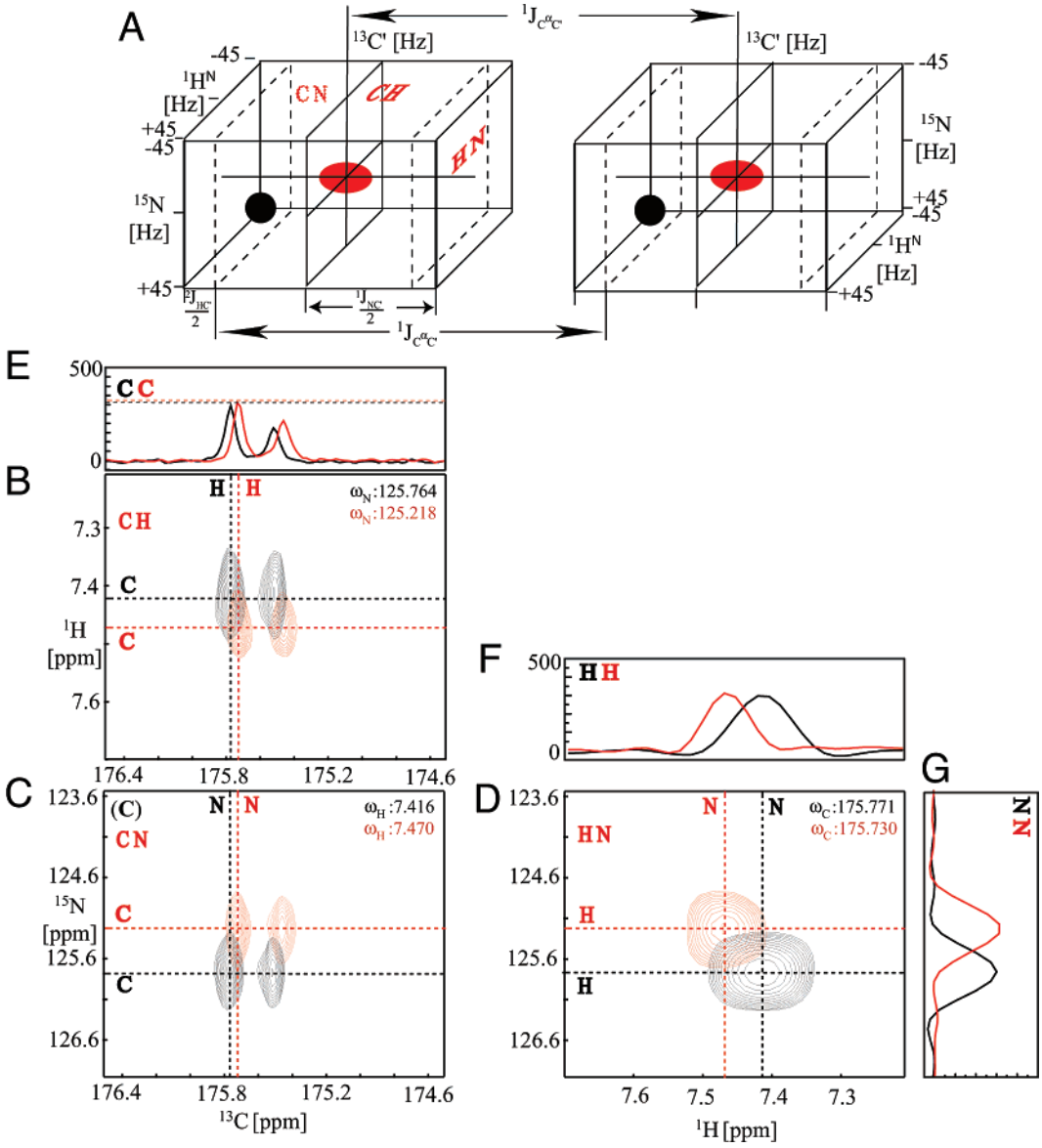

Figure 2. Three-dimensional c-TROSY−HNCO and c-HNCO spectra. (A) Schematic 3D representation of the position of a cross-peak in the 3D c-TROSY−HNCO spectrum (black) relative to that in a 3D c-HNCO spectrum (red). CN, CH, and HN are the three orthogonal planes. *J* couplings are not shown in proportion to their real values. (B−E) Experimental spectra recorded on ^{15}N/^{13}C/^{2}H/[Leu,Val]-methyl-protonated IIB^{Man}. (B−D) show the overlaid C′−H^{N}, C′−N, and H^{N}−N planes taken from the 3D c-TROSY−HNCO (black) and 3D c-HNCO (red) spectra for the H^{N}−N(Asp159)−C′(Thr158) cross-peaks at different chemical shifts in the third dimension indicated at the top-right corner of each panel. (E−G) show the aligned 1D slices through the H^{N}−N(Asp159)−C′(Thr158) cross-peaks along the directly detected C′ dimension, and the indirectly detected H^{N} and N dimensions, respectively. Slices are taken from (B−D) as indicated by the dashed lines. Spin-state selectivity in all dimensions in the 3D c-TROSY−HNCO experiment (see the text) is demonstrated by the observed chemical shift difference between the cross-peaks in the c-TROSY−HNCO and c-HNCO spectra in all three dimensions. The theoretical difference corresponds to $+J_{HN}/2$ (N$^{(\alpha)}$ state), $-J_{HN}/2$ (H$^{(\alpha)}$ state), (note γ_N is negative) and $-J_{NC'}/2 + J_{HC'}/2$ (N$^{(\beta)}$ state and H$^{(\alpha)}$ state) in H^{N}, N, and C′ dimensions, respectively. Note that J_{HN} and $J_{NC'}$ are negative. Dashed lines in (E) show the peak intensity in the 3D c-TROSY−HNCO (black) and c-HNCO (red) spectra with normalized noise levels. These data indicate that the experimental S/N ratio for the c-TROSY−HNCO, $(S/N)_{C-Trosy}$, is comparable to that of c-HNCO, $(S/N)_{C-HNCO}$, recorded on ^{15}N/^{13}C/^{2}H/[Leu,Val]-methyl-protonated IIB^{Man} ($\tau_c \approx 10$ ns at 30 °C).

pulse sequence to a nonconstant time version while still maintaining TROSY and sensitivity enhancement properties is feasible by changing phase cycles to select + or − spin order (stored separately) for every t_1 ($^{1}H_N$) point. Changing the $^{1}H_N$ (t_1) dimension from constant time to nonconstant time results in an improvement in S/N given by

$$\frac{(S/N)_{non-ct}}{(S/N)_{ct}} = \frac{(1 - e^{R \cdot t_{max}})}{R \cdot t_{max} \cdot e^{-R \cdot t}}$$

where R is the transverse relaxation rate of $^{1}H_N$. Assuming the constant time period $T = t_{max}$, the S/N improvement is given by $((e^{R \cdot T} - 1)/(R \cdot T))$, which depends on the product of RT. That is, when the transverse relaxation rate of $^{1}H_N$ is high, such as in a protein with a paramagnetic center or the presence of extensive NH water exchange, ^{1}H-detection will suffer severe sensitivity loss, while the nonconstant time version of the c-TROSY−HNCO will bring obvious advantages.

Theoretical Signal-to-Noise Analysis: 3D c-TROSY−HNCO versus 3D c-HNCO. The S/N ratio for a detected NMR signal can be estimated by multiplying the signal relaxation factors of the relevant product operators during all elements on

the coherence pathway by a factor f (accounting for number of scans, nuclei detection sensitivity, spin-state selectivity, and acquisition mode), a constant C (reflecting sample and hardware properties), and the product of the square roots of the number of time domain data points (TD) in all dimensions as:

$$\mathrm{S/N} \cong C\cdot f\cdot\prod_{i}^{\mathrm{ct}} \mathrm{e}^{-R_i T_i}\prod_{j}^{\text{non-ct}}\frac{1-\mathrm{e}^{-R_j\cdot t_{\max,j}}}{R_j\cdot t_{\max,j}}\prod_{k}\sqrt{TD_k} \quad (6)$$

where $\mathrm{e}^{-R_iT_i}$ is the signal scaling factor due to relaxation during a constant time element (ct, including the chemical shift constant time encoding period and the coherence transfer period of fixed duration) with relaxation rate R_i and duration T_i, and the scaling factor $((1-\mathrm{e}^{-R_j\cdot t_{\max,j}})/(R_j\cdot t_{\max,j}))$ is the S/N decay due to relaxation during a nonconstant time element (non-ct) j. In some pulse sequence elements, several different product operators contribute to the final NMR signal, and these product operators decay with different relaxation rates, for example during the ST2-PT and COS-S^3 transfer periods. In such cases, the relaxation rate is calculated as the average of the relaxation rates of the product operators involved.

The S/N for the ^{13}C-detected c-TROSY–HNCO (with subscript C-Trosy) and the ^{13}C-detected non-TROSY optimized HNCO (with subscript C-HNCO) experiments can be expressed as follows (with the signal relaxation factors arranged according to the order of the relevant product operators along the coherence pathway):

$$\begin{aligned}(\mathrm{S/N})_{\mathrm{C-Trosy}} \propto f_{\mathrm{C-Trosy}}\cdot\exp(-R^{\pm}_{HN(\alpha)}\cdot 2T_1)\cdot\\ \exp[-(\overline{RN^{N}_{H\pm}}+R_{MQ(HN,N)})/2)\cdot 2\tau]\cdot\exp[-(\overline{R^{H}_{N\pm}}+\\ R_{MQ(HN,N)})/2)\cdot 2\tau]\cdot\exp[-\overline{R^{C,C^{\alpha}}_{N\pm H(\alpha)}}\cdot 2T_2]\cdot\exp[-(\overline{R^{N,C^{\alpha}\pm}_{C\pm H^{\alpha}}}+\\ R_{MQ(C,N)H^{\alpha}})/2)\cdot 2T]\cdot\frac{1-\exp(-\overline{R^{C^{\alpha}}_{C-H(\alpha)N(\beta)}}\cdot t_{\mathrm{acq}})}{\overline{R^{C^{\alpha}}_{C-H(\alpha)N(\beta)}}\cdot t_{acq}} \quad (7)\end{aligned}$$

$$\begin{aligned}(S/N)_{C-HNCO} \propto f_{C-HNCO}\cdot\exp(-\overline{R^{N}_{H\pm}}\cdot 2T_1)\cdot\\ \exp[-\overline{R^{H,C,C^{\alpha}}_{N\pm}}\cdot(2T_2+2\tau)]\cdot\\ \exp(-\overline{R^{N,C^{\alpha}}_{C\pm}}\cdot 2T)\cdot\frac{1-\exp(-\overline{R^{H,N,C^{\alpha}}_{C-}}\cdot t_{acq})}{\overline{R^{H,N,C^{\alpha}}_{C-}}\cdot t_{acq}} \quad (8)\end{aligned}$$

where $2T_1$ and $2T_2$ are the ^{1}H and ^{15}N constant time evolution periods, respectively, set to 7.0 and 20 ms (which can be varied, depending on the required resolution and considerations of relaxation and INEPT transfer efficiency); 2τ is 5.3 ms; $2T_{NC}$ and $2T$ are set to be $(2T_2+2\tau)$ and 35 ms, respectively, counting the ^{15}N to ^{13}C′ forward and backward INEPT transfer times. $f_{\mathrm{C-Trosy}}$, and $f_{\mathrm{C-HNCO}}$ are the products of factors including number of scans (NS), nuclei detection sensitivity, spin-state selectivity, and acquisition mode given by:

$$f_{\mathrm{C-Trosy}} = \sqrt{NS}\cdot 1/8\cdot(1/2\cdot 1/2)\cdot(\sqrt{2}\cdot\sqrt{2}) \quad (9)$$

$$f_{\mathrm{C-HNCO}} = \sqrt{NS}\cdot 1/8 \quad (10)$$

where the factor of 1/8 is the nucleus detection sensitivity on ^{13}C instead of ^{1}H ($(\gamma_C/\gamma_H)^{3/2}\approx 1/8$); the factor 1/2 accounts for the selectivity of the spin state of ^{1}H or ^{15}N compared to spin-state nonselective detection; and the factor $\sqrt{2}$ is the sensitivity-enhancement factor obtained from the echo-antiecho acquisition mode for quadrature detection in ^{1}H and/or ^{15}N dimensions relative to a non-sensitivity-enhanced acquisition mode. Hereafter, for S/N comparisons, we assume that the sample and hardware properties (constant C), the number of time domain data points (TD_k) in a specific dimension k, and NS are same in both experiments. It is noteworthy that in the 3D c-TROSY–HNCO experiment, double echo–antiecho (dEA) acquisition is used for quadrature detection in both ^{1}H and ^{15}N dimensions, which gives a total of $\sqrt{2}\cdot\sqrt{2}=2$ times sensitivity enhancement.

In eqs 7 and 8, the relaxation rates for the single-transition product operators are calculated from eqs A1 and A2 provided in the Appendix in Supporting Information, in which the auto-correlated relaxation rates of the $^1/_2$ spins are calculated as described in ref 37 and the cross-correlated relaxation rates are calculated from eqs A3 and A7, depending on the properties of the CSA* tensor. Equation A3 is suitable for a general axially asymmetric CSA* tensor (such as carbonyl CSA* tensor), while the simplified eq A7 can be used for an approximately axially symmetric tensor (such as ^{15}N and ^{1}H CSA* tensors). The relaxation due to dipolar interaction with deuterons, such as ^{2}H$^{\alpha}$ and ^{2}H$^{\beta}$, in a perdeuterated sample, is scaled down by a factor of $8/3\times(\gamma_D/\gamma_H)^2\approx 1/16$ compared to that due to dipolar interaction with protons at the same positions.[38] However, this effect is very small. In our simulations, isotropic tumbling is assumed, and the following mechanisms causing relaxation are considered: CSA of ^{1}H^N, ^{15}N, and ^{13}C′; dipole/dipole interactions of ^{1}H$^N(i)$/^{15}N(i), ^{1}H$^N(i)$/^{1}H$^N(i+1)$, ^{1}H$^N(i)$/^{2}H$^{\alpha}(i)$, ^{1}H$^N(i)$/^{2}H$^{\alpha}(i+1)$, ^{1}H$^N(i)$/^{2}H$^{\alpha}(i+3)$, ^{1}H$^N(i)$/^{2}H$^{\beta}(i)$, ^{15}N(i)/^{13}C$^{\alpha}(i)$, ^{15}N(i)/^{13}C′$(i-1)$, ^{13}C′(i)/^{13}C$^{\alpha}(i)$, and ^{1}H$^N(i)$/^{13}C′$(i-1)$; and all corresponding cross-correlations between them. Standard expressions for the relaxation rates[37] and typical geometrical parameters are used (see Figure 3 legend). We also note the following features: (i) During the COS-S^3 element, the relevant product operators, both single-quantum operator ($C_{\pm}H^{(\alpha)}$) and multiple-quantum operator ($MQ_{(C,N)}H^{(\alpha)}$) are completely TROSY optimized with respect to the amide proton. (^{1}H^N is in the relaxation favorable α-state.) (ii) In the 3D c-TROSY–HNCO experiment, the directly detected operator on carbonyl $C_{-}H^{(\alpha)}N^{(\beta)}$ is TROSY optimized with respect to both the amide proton and nitrogen. (^{1}H^N is in the relaxation favorable α-state, and ^{15}N is in the relaxation favorable β-state.) The doubly TROSY optimized carbonyl relaxation rate typically decreases by 15% for proteins with a correlation time larger than 20 ns (see Figure S1, Supporting Information). However, the nonuniform CSA* tensor of the carbonyl results in a rather disperse relaxation attenuation. (iii) The limiting factor for the carbon detected c-TROSY–HNCO experiment is the dominant relaxation due to the large carbonyl CSA* with $\Delta\sigma_{CO}\approx 130$ ppm (given by $\Delta\sigma_S=\sigma_{S,\parallel}-\sigma_{S,\perp}=\sigma_{S,ZZ}-(\sigma_{S,XX}+\sigma_{S,YY})/2$). The relaxation rates become approximately linearly proportional to the square of the polarizing field. This implies that these experiments could have even higher S/N ratio at low polarizing field, although this would compromise the TROSY effect in the ^{1}H^N and ^{15}N

(37) Korzhnev, D. M.; Billeter, M.; Arseniev, A. S.; Orekhov, V. Y. *Prog. Nucl. Magn. Reson. Spectrosc.* **2001**, *38*, 197–266.
(38) Mal, T. K.; Matthews, S. J.; Kovacs, H.; Campbell, I. D.; Boyd, J. *J. Biomol. NMR* **1998**, *12*, 259–276.

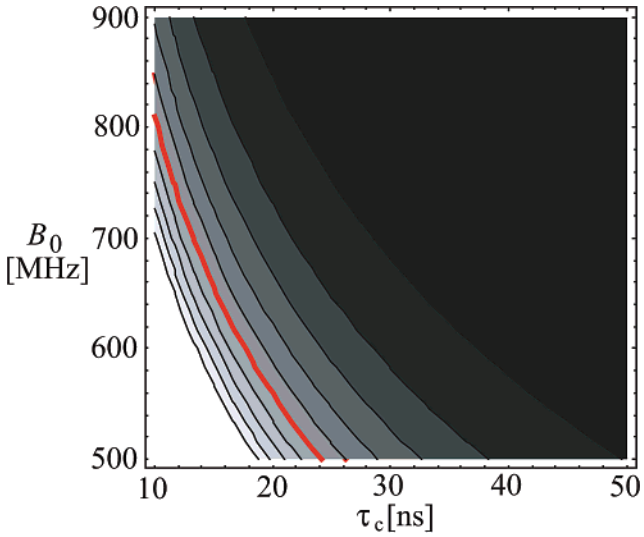

Figure 3. Contour plot of S/N ratio for the ^{13}C-detected c-TROSY−HNCO experiment versus B_0 and τ_c. The relative scale is arbitrary. The red curve is the equidistance line corresponding to the experimental S/N ratio observed for the 0.75 mM sample of ^{15}N/^{13}C/^{2}H/ [Leu,Val]-methyl-protonated IIB^{Man}. The following parameters were used for the S/N ratio simulations. The chemical shielding anisotropy (CSA*) tensors of H and N were assumed to be symmetric with $\Delta\sigma_{H^N} = +8$ ppm, $\Delta\sigma_N = -170$ ppm; the angles between the N−H bond and the tensor main axes are $\theta^{HN,\Delta\sigma H^N} = 0°$ and $\theta^{HN,\Delta\sigma N} = 15°$. The carbonyl CSA* tensor is highly asymmetric with $\sigma_{C',XX} = -73$ ppm, $\sigma_{C',YY} = -15$ ppm, and $\sigma_{C',ZZ} = 88$ ppm; the angles between the N−C′ bond and the axes are $\theta^{NC',XX_{\sigma C'}} = 40°$, $\theta^{NC',YY_{\sigma C'}} = 130°$, and $\theta^{NC',ZZ_{\sigma C'}} = 90°$, and the angles between the H^N−C′ bond and the axes are $\theta^{HNC',XX_{\sigma C'}} = 70°$, $\theta^{HNC',YY_{\sigma C'}} = 160°$, and $\theta^{HNC',ZZ_{\sigma C'}} = 90°$.[47] The bond lengths are $r_{HN} = 1.04$ Å, $r_{HC} = 1.09$ Å and $r_{CC} = 1.53$ Å. The intra- and interresidue distances correspond to those in α helices and turns:[48] $r_{H^NH^N} = 2.70$ Å, $r_{H^NH^\alpha(i)} = 3.50$ Å, $r_{H^NH^\alpha(i+1)} = 3.50$ Å, $r_{H^NH^\alpha(i+3)} = 3.40$ Å, $r_{H^NH^\beta} = 3.00$ Å, $r_{NC'} = 1.33$ Å, $r_{H^NC^\alpha} = 1.47$ Å, and $r_{H^NC'} = 2.00$ Å.

dimensions. Figure 3 shows a contour plot of S/N ratio for the ^{13}C-detected c-TROSY−HNCO experiment versus the polarizing field B_0 and the correlation time τ_c. For a specific desired S/N value, τ_c can increase (that is, the molecular mass becomes larger) with decreasing B_0. For example, the S/N ratio obtained experimentally at 800 MHz for the 18.6 kDa ^{15}N/^{13}C/^{2}H/-[Leu,Val]-methyl-protonated IIB^{Man} sample (0.75 mM, $\tau_c \approx 10$ ns at 30 °C) can be achieved for a protein with a correlation time of 25 ns (at 30 °C, equivalent to a molecular mass of ∼46 kDa) if the experiment is run at 500 MHz, as indicated by the red curve in Figure 3. Figure 4 shows a comparison of the S/N ratios for the c-TROSY−HNCO and c-HNCO experiments. Even though only one-fourth of the initial magnetization is transferred to carbonyl for detection in the TROSY-based experiment, the S/N ratio for proteins with a correlation time of 10 ns or larger is in fact comparable to or even higher than that of the c-HNCO experiment due to more favorable relaxation properties in all dimensions (cf. the experimental data on IIB^{Man} shown in Figure 2E).

Application to Measurement of $^1J_{C^\alpha C'}$ ($^1D_{C^\alpha C'}$). The high resolution in the directly detected ^{13}C′ dimension afforded by the c-TROSY−HNCO and c-HNCO experiments permits the observation of the doublet splitting due to the $^1J_{C^\alpha C'}$ scalar coupling in an isotropic medium or to the sum of the C$^\alpha$−C′ one-bond scalar and dipolar couplings, $^1J_{C^\alpha C'}+{}^1D_{C^\alpha C'}$, in a weak alignment medium. This suggests that these experiments can be used to accurately measure $^1D_{C^\alpha C'}$ RDCs from the difference in the doublet splitting observed in anisotropic and isotropic media. Indeed, carbon-detected spectroscopy has been proposed

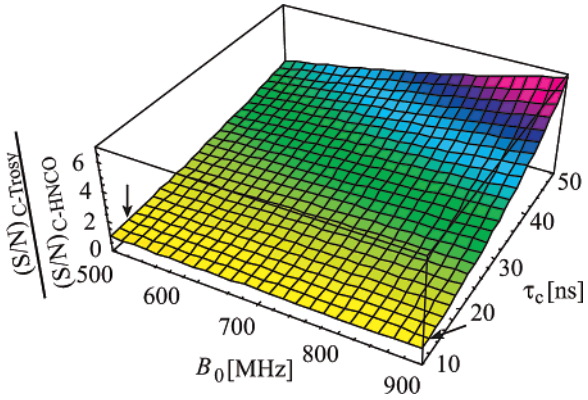

Figure 4. Theoretical comparison of the S/N ratios for ^{13}C-detected HNCO experiments, $(S/N)_{C-Trosy}/(S/N)_{C-HNCO}$, versus the polarizing field B_0 and correlation time τ_c. Dark-orange squares (black arrows) indicate (B_0,τ_c) sets with $(S/N)_{C-Trosy}/(S/N)_{C-HNCO} \approx 1$. The S/N ratio is calculated using the same parameters as in Figure 3.

for measurement of side-chain ^{13}C−^{13}C RDCs,[39] and very recently for measurement of C$^\alpha$−C′, C$^\alpha$−C$^\beta$, and even H^N−N and H$^\alpha$−C$^\alpha$, RDCs in the 9 kDa protein calbindin D$_{9K}$ with one of the calcium sites substituted by a paramagnetic lanthanide.[40] The relationship $\Delta D = LW/(S/N)$, where LW is the line width in the directly detected carbon dimension, can be used to approximate the lower limit for the uncertainty of the measured RDCs.[41,42] Assuming a Lorentzian line shape, LW is proportional to the relaxation rates of $R^{C\alpha}_{C-H(\alpha)N(\beta)}$ and R^{H,N,C^α}_{C-} for the c-TROSY−HNCO and c-HNCO experiments, respectively. $(S/N)_{C-Trosy}$ and $(S/N)_{C-HNCO}$ can be calculated from eqs 7 and 8. Simulations indicate that the c-TROSY−HNCO experiment yields higher precision (lower uncertainty) compared to the c-HNCO experiment as the molecular weight of the macromolecule increases (Figure 5). Selecting TROSY-optimized components in all dimensions in the c-TROSY−HNCO experiment therefore makes it ideal for RDC measurements in large macromolecules. In the case of ^{15}N/^{13}C/^{2}H/[Leu,Val]-methyl-protonated IIB^{Man}, the experimental pairwise rmsd for the 114 measured $^1J_{C^\alpha C'}$ couplings (excluding overlapped cross-peaks and cross-peaks with shape distortion) measured from two independent experiments, is 0.77 Hz. In contrast to quantitative *J* correlation methods for the measurement of $^1D_{C^\alpha C'}$ RDCs,[42] the c-TROSY−HNCO and c-HNCO experiments directly measure the doublet splitting and are therefore expected to be more tolerant to nonuniform values of $^1J_{C^\alpha C'}$ (or $^1J_{C^\alpha C'} + {}^1D_{C^\alpha C'}$ for aligned samples) and thus not strictly limited by alignment strength. Thus, considering that the magnitude of $^1D_{C^\alpha C'}$ is approximately one-fifth that of $^1D_{NH}$,[43] the degree of alignment can be increased significantly relative to that used for the measurement of $^1D_{NH}$, thereby increasing the size and therefore the relative accuracy of the $^1D_{C^\alpha C'}$ RDC couplings. In addition, the measured $^1D_{C^\alpha C'}$ RDCs in the c-TROSY−HNCO experiment should not be affected by incomplete ^{13}C labeling and will be less affected by small passive couplings and pulse imperfections

(39) Vogeli, B.; Kovacs, H.; Pervushin, K. *J. Am. Chem. Soc.* **2004**, *126*, 2414−2420.
(40) Balayssac, S.; Bertini, I.; Luchinat, C.; Parigi, G.; Piccioli, M. *J. Am. Chem. Soc.* **2006**, *128*, 15042−15043.
(41) Kontaxis, G.; Clore, G. M.; Bax, A. *J. Magn. Reson.* **2000**, *143*, 184−196.
(42) Jaroniec, C. P.; Ulmer, T. S.; Bax, A. *J. Biomol. NMR* **2004**, *30*, 181−194.
(43) Bax, A.; Kontaxis, G.; Tjandra, N. *Methods Enzymol.* **2001**, *339*, 127−174.

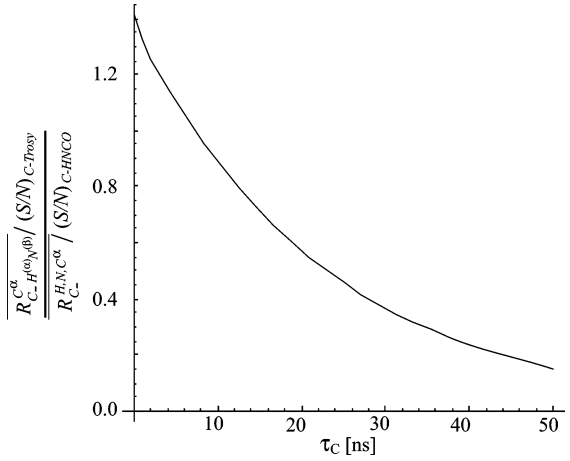

Figure 5. Theoretical comparison of the precision of the measured $^1D_{C^\alpha C'}$ RDC couplings using c-TROSY−HNCO and c-HNCO experiments as a function of the correlation time τ_c of the macromolecule. Here $\Delta D = \mathrm{LW}/(\mathrm{S/N})$ is used to approximate the lower limit for the uncertainty of the measured dipolar couplings.[41,42] LW is the line width in the carbon dimension. With the assumption of a Lorentzian line shape, LW is proportional to the relaxation rates of $\overline{R_{C^-}^{H,N,C^\alpha}}$ and $\overline{R_{C^-H^{(\alpha)}N^{(\beta)}}^{C^\alpha}}$ for c-HNCO and c-TROSY−HNCO, respectively. Relaxation rates are calculated at 800 MHz.

compared to quantitative *J* correlation methods[42] due to the smaller number of pulses applied in the out-and-stay coherence transfer used in the c-HNCO−TROSY experiment.

Concluding Remarks

In this paper, we have presented a carbon-detected triple resonance experiment, c-TROSY−HNCO, with TROSY optimization in all dimensions and sensitivity enhancement in both indirect dimensions. The $^1H^N$ and ^{15}N TROSY effects are maintained in both indirect dimensions, while the directly detected $^{13}C'$ is doubly TROSY-optimized with respect to $^1H^N$ and ^{15}N. In addition, a new, generally applicable, sensitivity enhancement method, the so-called double echo−antiecho (dEA), is described that provides sensitivity enhancement of $\sqrt{2}$ in both indirect dimensions.

The c-HNCO−TROSY experiment can be used to accurately measure $^1D_{C^\alpha C'}$ RDCs in the direct carbon dimension. Selecting TROSY-optimized components in all dimensions makes it suitable for application to large-sized proteins. Selection of the detected carbon under a single spin state with respect to H^N and N offers high resolution and concomitantly high precision for the measurement of RDCs. If the spin state with respect to H^N or N is swapped, which can be achieved simply by applying an additional H^N or N 180° pulse immediately prior to carbon detection, $^2J_{HC'}$ ($^2D_{HC'}$) or $^1J_{NC'}$ ($^1D_{NC'}$) couplings can also be measured. Compared to quantitative *J* correlation methods for the measurement of $^1D_{C^\alpha C'}$,[42] directly measuring the doublet splitting is expected to be more tolerant to nonuniform $^1J_{C^\alpha C'}$ (or $^1J_{C^\alpha C'} + {}^1D_{C^\alpha C'}$ for aligned samples). In addition, the out-and-stay coherence transfer in the c-HNCO−TROSY experiment uses a smaller number of INEPT elements relative to conventional ^{1}H-detected out-and-back experiments which is advantageous since each additional INEPT element can lead to additional signal loss due to nonuniform effective one-bond couplings (which is especially the case in an anisotropic medium). Finally, the doublet arising from the $^1J_{C^\alpha C'}$ coupling can also be converted to a single cross-peak with even higher S/N ratio by applying band selective homodecoupling[44] during acquisition or by appropriate deconvolution during signal processing.[45]

The design principles of the c-TROSY−HNCO experiment are quite general and can be readily extended to other experiments, such as a c-HNCA-TROSY experiment. Because the CSA of C^α is smaller than that of C', considerations of carbon relaxation suggest that detection of C^α can be advantageous, especially at high fields where relaxation due to CSA is dominant. In designing a c-HNCA-TROSY experiment, it should be borne in mind that $N/C^\alpha(i, i-1)$ is an IS_2 spin system (instead of *IS*) due to *J* coupling of ^{15}N to both the intra- and interresidue C^α and that the passive coupling of C^α to C^β could potentially lead to some signal loss during the COS-S^3 element.

Acknowledgment. We thank Ad Bax for useful discussions. B.V. acknowledges a Fellowship from the Swiss National Science Foundation. This work was supported by the intramural program of the NIH, NIDDK, and by the AIDS Targeted Antiviral Program of the Office of the Director of the NIH (to G.M.C.).

Supporting Information Available: Appendix providing uniform definition of single-transition product operators and the corresponding formulas to calculate their relaxation rates as applied throughout this manuscript; one figure providing a comparison of carbonyl relaxation as a function of correlation time for c-TROSY−HNCO and c-HNCO experiments; and one figure providing an experimental comparison of the signal-to-noise ratios for the c-TROSY−HNCO and conventional ^{1}H-detected TROSY−HNCO experiments. This material is available free of charge via the Internet at http://pubs.acs.org.

JA067981L

(44) Vogeli, B.; Kovacs, H.; Pervushin, K. *J. Biomol. NMR* **2005**, *31*, 1−9.
(45) Shimba, N.; Stern, A. S.; Craik, C. S.; Hoch, J. C.; Dotsch, V. *J. Am. Chem. Soc.* **2003**, *125*, 2382−2383.
(46) Marion, D.; Ikura, M.; Tschudin, R.; Bax, A. *J. Magn. Reson.* **1989**, *85*, 393−399.
(47) Cornilescu, G.; Bax, A. *J. Am. Chem. Soc.* **2000**, *122*, 10143−10154.
(48) Wuthrich, K. *NMR of Proteins and Nucleic Acids*; Wiley: New York, 1986.